

Formation of Bound States in Quintessence Alternative Theories

George Koutsoumbas,^{1,*} Andri Machattou,^{1,†} and Eleftherios Papantonopoulos^{1,‡}

¹*Physics Division, School of Applied Mathematical and Physical Sciences,
National Technical University of Athens, 15780 Zografou Campus, Athens, Greece.*

(Dated: June 27, 2025)

We study the formation and behaviour of bound states formed outside the horizon of a black hole in the presence of quintessence matter. Calculating the Regge and Wheeler potential for general metric function, we find that the presence of quintessence influences significantly the metric function and the Hawking temperature. We show that large black holes radiate less in the presence of large quintessence matter and it seems to live longer, while small black holes radiate more.

Contents

I. Introduction	2
II. Generalized Regge-Wheeler Potential	3
III. Quintessence Matter and its Thermodynamics	4
A. Description of the Quintessence	5
B. Thermodynamics in AdS Spacetime	5
IV. Regge-Wheeler potentials	7
V. Formation of Bound States	8
VI. Conclusions	10
References	10

arXiv:2506.21097v1 [gr-qc] 26 Jun 2025

*Electronic address: kutsubas@central.ntua.gr

†Electronic address: andrimachattou@hotmail.com

‡Electronic address: lpapa@central.ntua.gr

I. INTRODUCTION

Bound states for particles around black holes is a very interesting effect and a detailed study was carried out in [1]. A similar study can be done by the investigation of QNMs. In both cases the goal is to find the characteristic complex frequencies for a scalar field which propagates in a black hole background. The constraints which the scalar field has to satisfy are boundary conditions at the black hole horizon and at spatial infinity. However, the physical meanings of bound states and quasi-normal modes are very different and correspond to different energy ranges. In [1] a systematic study was carried out of quanta trapped between the finite black hole potential barrier and the infinitely thick well which works as a barrier preventing the particles from reaching infinity. These bound states may have possible cosmological consequences related to the primordial power spectrum [2, 3]. Also the phenomenology of these bound states and their spectra should be studied in details and experiments associated with light black holes should also take into account those states.

One basic tool to examine the stability of a black hole is to study the Regge and Wheeler potential. Regge and Wheeler [4] first described a decomposition of perturbations on a spherically symmetric background geometry into tensor harmonics and wrote the perturbation equations in terms of these harmonics. They found that it is possible to put the equations for the oscillatory motion into the form of a single second-order Schrodinger-type differential equation with an effective potential. Then the study of these equations can give us important information on the stability of the black hole. The first metric that was studied by Regge and Wheeler was the Schwarzschild metric.

The formation and propagation of quantum bound states in the vicinity of a Galileon black hole was discussed in [6]. The Galileon black holes are generated by a scalar field coupled to the Curvature [7–9] and they are spherically symmetric hairy black holes. Classically this coupling has been studied extensively; it strongly influences the propagation of the scalar field compared to a scalar field minimally coupled to gravity. Also the stability of the background Galileon black hole was studied and it was found that bound states were trapped in a Regge and Wheeler potential well or penetrating the horizon of the Galileon black hole depending on the strength of the derivative coupling of a scalar field to curvature. The formation of quantum bound states requires that the Klein-Gordon equation in a black hole background has to exhibit a radial potential containing a local well for given ranges of black hole parameters.

Recent astronomical observations suggest that our Universe is expanding at an accelerating rate [10, 11]. Responsible for this expansion is the dark sector of our Universe consisting mainly of dark energy, while the presence of a cosmological constant cannot explain this expansion [12, 13]. Approximately 70% of the energy density in the universe is in the form of an exotic, negative-pressure component, dubbed dark energy. The observational bounds on the properties of the dark energy have continued to tighten. Taking w to be the ratio of pressure to density for the dark energy $w = p_{DE}/\rho_{DE}$, recent observational constraints the range of $-1 \leq w \leq -\frac{1}{3}$, which causes the acceleration. The border case of $w = -1$ of the extraordinary quintessence covers the cosmological constant term. As it was recognized [14–16], the acceleration represents a challenge for the consistent theory of quantum gravity, because of the outer horizon, which does not allow one to introduce the observable S-matrix in terms of asymptotic past and future states. The outer horizon of de Sitter space significantly differs from the inner horizon of black hole, which has asymptotically flat space far away from the black hole.

The presence of a quintessence field to explain the Universe expansion modifies General Relativity and new modified Gravity theories were proposed with the presence of dynamical scalar fields [17]. In these theories black hole solutions were found in the presence of the quintessence matter field. One of the first black hole solution in the presence of quintessence was discussed in [18]. New static spherically-symmetric exact solutions of Einstein equations with the quintessential matter surrounding a black hole charged or uncharged were presented. A condition of additivity and linearity in the energy-momentum tensor was found which allows to get correct limits to the known solutions for the electromagnetic static field. Further studies in the presence of quintessence matter were carried out and new black holes solutions were obtained, and the impacts of the quintessence field on their thermal quantities, shadows, and quasinormal modes were discussed [19]–[26]. The presence of dark matter and quintessence fields outside the horizon of a black hole has an impact on their thermodynamic properties, such as the temperature, and introduces new critical phenomena. These modifications could lead to generalizations of classical thermodynamic results making this area of study very interesting leading to connection between a black hole event horizon and its entropy [27, 28].

The aim of this work is to study the formation and behaviour of bound states formed outside the horizon of a hairy black hole in which the hair is formed by a quintessence matter. Then considering a general form of the metric function we derive a Schrödinger equation in which the Regge and Wheeler potential appears. Considering also the thermodynamics of the solution we discuss the formation and the behaviour of the bound states formed for various values of the quintessence parameter w .

The work is organized as follows. In section II we review the Regge-Wheeler potential for a fairly general metric function. In section III the quintessence is introduced and some aspects of its thermodynamics are described. Section IV deals with the Regge-Wheeler potential for scalar excitations, while in section V mass eigenstates are calculated. Section VI contains our conclusions.

II. GENERALIZED REGGE-WHEELER POTENTIAL

In this Section we will consider a fairly general metric and we will calculate the Regge-Wheeler potential, following [5]. We consider the metric:

$$ds^2 = -G(r)dt^2 + \frac{dr^2}{F(r)} + H(r)d\Omega^2 . \quad (1)$$

Then particles with spin s satisfy equation:

$$\begin{aligned} & -\frac{H}{G}\partial_{tt}\Psi_s(t, r, \theta, \phi) + s\sqrt{\frac{F}{G}}\left(H\frac{G'}{G} - H'\right)\partial_t\Psi_s(t, r, \theta, \phi) + FH\partial_{rr}\Psi_s(t, r, \theta, \phi) \\ & + \left(\frac{F'H}{2} + \left(s + \frac{1}{2}\right)\frac{FG'H}{G} + (s+1)FH'\right)\partial_r\Psi_s(t, r, \theta, \phi) \\ & + \left[\frac{1}{\sin\theta}\partial_\theta(\sin\theta\partial_\theta) + \frac{2is\cot\theta}{\sin\theta}\partial_\phi + \frac{1}{\sin^2\theta}\partial_{\phi\phi} - s - s^2\cot^2\theta\right]\Psi_s(t, r, \theta, \phi) \\ & + \left[s\frac{FG''H}{G} + \frac{3s-2s^2}{2}FH'' - \frac{s}{2}\frac{FG'^2H}{G^2} + \frac{2s^2-s}{4}\frac{FH'^2}{H} + \frac{s}{2}\frac{F'G'H}{G}\right. \\ & \left. + \frac{3s-2s^2}{2}F'H' + \frac{2s^2+5s}{4}\frac{FG'H'}{G}\right]\Psi_s(t, r, \theta, \phi) = 0 . \end{aligned} \quad (2)$$

We decompose the various fields into radial, spherical and time parts, using the ansatz

$$\Psi_s(t, r, \theta, \phi) = R_s(r)\mathcal{Y}_{lm}^s(\theta, \phi)e^{-i\omega t} , \quad (3)$$

where $\mathcal{Y}_{lm}^s(\theta, \phi)$ are the generalized spherical harmonics with spin s , which satisfy the equation

$$\left[\frac{1}{\sin\theta}\partial_\theta(\sin\theta\partial_\theta) + \frac{2is\cot\theta}{\sin\theta}\partial_\phi + \frac{1}{\sin^2\theta}\partial_{\phi\phi} - s - s^2\cot^2\theta + \lambda_l^s\right]\mathcal{Y}_{lm}^s(\theta, \phi) = 0 , \quad \lambda_l^s = l(l+1) - s(s+1) . \quad (4)$$

The radial part of the wavefunction will then satisfy:

$$A_s(B_s R'_s)' + \left(\frac{\omega^2 H}{G} + i\omega s\sqrt{\frac{F}{G}}\left(H\frac{G'}{G} - H'\right) + C_s\right)R_s = 0, \quad A_s = \sqrt{\frac{F}{G}}\frac{1}{(GH)^s}, \quad B_s = H\sqrt{FG}(GH)^s , \quad (5)$$

$$\begin{aligned} C_s = & s\frac{FG''H}{G} + \frac{3s-2s^2}{2}FH'' - \frac{s}{2}\frac{FG'^2H}{G^2} \\ & + \frac{2s^2-s}{4}\frac{FH'^2}{H} + \frac{s}{2}\frac{F'G'H}{G} + \frac{3s-2s^2}{2}F'H' + \frac{2s^2+5s}{4}\frac{FG'H'}{G} - \lambda_l^s - 2s . \end{aligned} \quad (6)$$

We will define

$$R_s \equiv \frac{u_s}{\sqrt{H}} ,$$

and then the radial part of the equation becomes:

$$\begin{aligned} A_s(B_s R'_s)' = & \frac{\sqrt{H}}{G}\left[FGu_s'' + \frac{1}{2}\frac{(FG)'u_s'}{G}\right] \\ & + \frac{1}{4}\left[\frac{FH'^2}{H} - F'H' - \frac{FG'H'}{G} - 2FH''\right]\frac{u_s}{\sqrt{H}} . \end{aligned} \quad (7)$$

Using the tortoise coordinate

$$\frac{d}{dr} = \frac{1}{\sqrt{FG}}\frac{d}{dr_*} , \quad (8)$$

we will get

$$\frac{du_s}{dr} = \frac{1}{\sqrt{FG}} \frac{du_s}{dr_*}, \quad \frac{d^2u_s}{dr^2} = \frac{1}{FG} \frac{d^2u_s}{dr_*^2} - \frac{(FG)'}{2(FG)^{3/2}} \frac{du_s}{dr_*}, \quad (9)$$

so that

$$A_s(B_s R'_s)' = \frac{\sqrt{H}}{G} \frac{d^2u_s}{dr_*^2} + \frac{1}{4} \left[\frac{FH'^2}{H} - F'H' - \frac{FG'H'}{G} - 2FH'' \right] \frac{u_s}{\sqrt{H}}, \quad (10)$$

and the radial equation takes a Schrödinger-like form.

$$-\frac{d^2u_s}{dr_*^2} + V_s u_s = \omega^2 u_s, \quad (11)$$

where the potentials for $s = 0, 1, 2, \frac{1}{2}$ read

$$V_0 = \nu_l^0 \frac{G}{H} + \frac{1}{\sqrt{H}} \frac{d^2}{dr_*^2} \sqrt{H} = \nu_l^0 \frac{G}{H} + \frac{1}{\sqrt{H}} \left[FG \frac{d^2 \sqrt{H}}{dr^2} + \frac{1}{2} \frac{d(FG)}{dr} \frac{d\sqrt{H}}{dr} \right], \quad (12)$$

$$V_1 = \nu_l^1 \frac{G}{H}, \quad (13)$$

$$V_2 = \nu_l^2 \frac{G}{H} + \frac{1}{2H^2} \left(\frac{dH}{dr_*} \right)^2 - \frac{1}{\sqrt{H}} \frac{d^2}{dr_*^2} \sqrt{H} = \nu_l^2 \frac{G}{H} + \frac{FG}{2H^2} \left(\frac{dH}{dr} \right)^2 - \frac{1}{\sqrt{H}} \left[FG \frac{d^2 \sqrt{H}}{dr^2} + \frac{1}{2} \frac{d(FG)}{dr} \frac{d\sqrt{H}}{dr} \right], \quad (14)$$

$$V_{\frac{1}{2}} = \nu_l^{1/2} \frac{G}{H} \pm \sqrt{\nu_l^{1/2}} \frac{d}{dr_*} \sqrt{\frac{G}{H}} = \nu_l^{1/2} \frac{G}{H} \pm \sqrt{\nu_l^{1/2} FG} \frac{d}{dr} \sqrt{\frac{G}{H}}, \quad \nu_l^s = l(l+1) - s(s-1). \quad (15)$$

In the case, where ($F=G=f$, $H = r^2$) with the metric

$$ds^2 = -f(r)dt^2 + \frac{dr^2}{f(r)} + r^2 d\Omega^2, \quad (16)$$

the potentials become

$$V_0 = f \left[\frac{l(l+1)}{r^2} + \frac{f'}{r} \right], \quad V_1 = l(l+1) \frac{f}{r^2}, \quad V_2 = f \left[\frac{l(l+1)-2}{r^2} - \frac{2f}{r^2} - \frac{1}{r} \frac{df}{dr} \right], \quad (17)$$

$$V_{\frac{1}{2}} = f \left[\frac{l(l+1) + \frac{1}{4}}{r^2} \pm \sqrt{l(l+1) + \frac{1}{4}} \frac{d}{dr} \sqrt{\frac{f}{r^2}} \right]. \quad (18)$$

As we can see the spin changes the structure of the Regge-Wheeler potential. In this work we concentrate on the $s = 0$ case.

III. QUINTESSENCE MATTER AND ITS THERMODYNAMICS

In this section we will introduce quintessence matter outside the horizon of a black hole and we study the thermodynamics of the coupling system and discuss the formation of bound states.

A. Description of the Quintessence

As we have already discussed quintessence is a scalar field, whose equation of state parameter w is defined as the ratio of its pressure p and its energy density ρ which is given by a kinetic term and a potential term as

$$w = \frac{p}{\rho} = \frac{\frac{1}{2}\dot{\phi}^2 - V(\phi)}{\frac{1}{2}\dot{\phi}^2 + V(\phi)}, \quad -1 \leq w \leq -\frac{1}{3}. \quad (19)$$

The energy-momentum tensor in the presence of quintessence is given by [18]:

$$T_t^t = \rho, \quad T_k^l = 3w\rho \left[-(1+3B)\frac{r_k r^l}{r^2} + B\delta_k^l \right], \quad B = -\frac{1+3w}{6w}. \quad (20)$$

Averaging over angles, taking into account that $\langle r_k r^l \rangle = \frac{1}{3}r^2\delta_k^l$, yields

$$\langle T_k^l \rangle = -p\delta_k^l. \quad (21)$$

Writing the line element in the form:

$$ds^2 = (1+h)dt^2 - \frac{dr^2}{1+h} - r^2 d\Omega^2 = f dt^2 - \frac{dr^2}{f} - r^2 d\Omega^2, \quad f \equiv 1+h, \quad (22)$$

the Einstein equations read:

$$T_t^t = -\frac{1}{2r^2}(h + rh') = \rho, \quad T_\theta^\theta = T_\phi^\phi = -\frac{1}{4r}(2h' + rh'') = -\frac{1}{2}\rho(3w+1). \quad (23)$$

There exist two solutions, the well-known Schwarzschild solution $h = -\frac{2M}{r}$ and a novel one

$$h = \frac{a}{r^{1+3w}}. \quad (24)$$

The Einstein equations yield:

$$\rho = \frac{a}{2} \frac{3w}{r^{3(w+1)}}, \quad R = 3aw \frac{1-3w}{r^{3(1+w)}}. \quad (25)$$

Notice that R is singular at $r \rightarrow 0$, except when $w = 0, \frac{1}{3}, -1$. Additivity and linearity yield the final solution for the metric: $f = 1 - \frac{2M}{r} - \frac{a}{r^{1+3w}}$. The generalized solution to the Reissner–Nordström–anti-deSitter black hole reads:

$$f = 1 - \frac{2M}{r} + \frac{Q^2}{r^2} + \frac{r^2}{L^2} - \frac{a}{r^{1+3w}}. \quad (26)$$

As we can see the metric function in the AdS space apart from the usual parameters of mass and charge because of the presence of quintessence matter also depends on two more parameters a and w , which, as we will discuss, play a crucial role in the thermodynamics of the system and the formation of bound states.

B. Thermodynamics in AdS Spacetime

The mass can be expressed in terms of the remaining parameters and the horizon, since $f(r_+) = 0$:

$$M = \frac{r_+}{2} \left[1 + \frac{Q^2}{r_+^2} + \frac{r_+^2}{L^2} - \frac{a}{r_+^{1+3w}} \right]. \quad (27)$$

The Hawking temperature is given by:

$$T = \frac{1}{4\pi} f'(r_+) = \frac{1}{4\pi} \left[\frac{2M}{r_+^2} - \frac{2Q^2}{r_+^3} + \frac{2r_+}{L^2} + \frac{a(1+3w)}{r_+^{2+3w}} \right], \quad (28)$$

and substituting the mass M it becomes:

$$T = \frac{\frac{3r_+}{L^2} - \frac{Q^2}{r_+^3} + \frac{1}{r_+^2}(r_+ + 3awr_+^{-3w})}{4\pi}, \quad (29)$$

while the entropy is given by

$$S = \int \frac{dM}{T} = \frac{A}{4} = \pi r_+^2. \quad (30)$$

In the following we will investigate how the above quantities are affected by the quintessence parameters a and w . We set $L = 1$.

In Fig. 1, upper left panel, we plot the metric function for $Q = 0.00$, $w = -0.80$ and various values of the a parameter. In the upper right panel of the same figure, we plot the metric function for $Q = 0.00$, $a = 0.80$ and various values of the w parameter. In the panel down left, we plot the metric function for $Q = 0.20$, $w = -0.80$ and various values of the a parameter. Finally, in the panel down right, we plot the metric function for $Q = 0.20$, $a = 0.80$ and various values of the w parameter. As we can see, the existence of a non-zero charge Q in the black hole tends to decrease the value of the metric function. The qualitative characteristics of the graphs do not change much with respect to the $Q = 0.00$ cases.

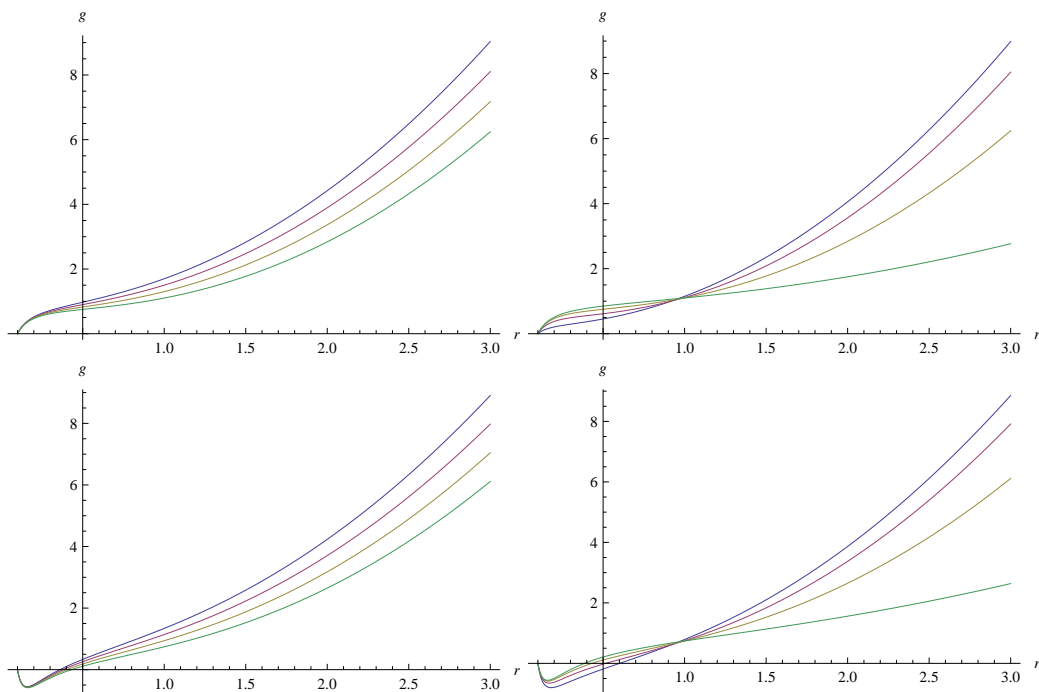


FIG. 1: (a) Metric function $g \equiv f(r)$ versus r for $Q = 0.00$, $w = -0.80$ and $a = 0.20$, (blue curve) $a = 0.40$ (purple curve) $a = 0.60$ (brown curve) and $a = 0.80$ (cyan curve). (b) Metric function $g \equiv f(r)$ versus r for $Q = 0.00$, $a = 0.80$ and $w = -0.40$, (blue curve) $w = -0.60$ (purple curve) $w = -0.80$ (brown curve) and $w = -1.00$ (cyan curve). (c) Metric function $g \equiv f(r)$ versus r for $Q = 0.20$, $w = -0.80$ and $a = 0.20$, (blue curve) $a = 0.40$ (purple curve) $a = 0.60$ (brown curve) and $a = 0.80$ (cyan curve). (d) Metric function $g \equiv f(r)$ versus r for $Q = 0.20$, $a = 0.80$ and $w = -0.40$, (blue curve) $w = -0.60$ (purple curve) $w = -0.80$ (brown curve) and $w = -1.00$ (cyan curve).

In Fig. 2, upper left panel, we plot the temperature versus r_+ for $Q = 0.00$, $w = -0.80$ and various values of the a parameter. In the upper right panel of the same figure, we plot the temperature versus r_+ for $Q = 0.00$, $a = 0.80$ and various values of the w parameter. In the panel down left, we plot the temperature versus r_+ for $Q = 0.20$, $w = -0.80$ and various values of the a parameter. Finally, in the panel down right, we plot the temperature versus r_+ for $Q = 0.20$, $a = 0.80$ and various values of the w parameter. As we can see, the existence of a non-zero charge Q in the black hole tends to decrease the value of the metric function.

The dependence of the temperature on a is monotonous, making it smaller for increasing a . This characteristic does not survive at $Q = 0.20$, as is obvious from the left panels of the figure.

The w dependence is less trivial: it is smaller for large r_+ , while for modest r_+ it is larger. For $Q = 0.00$, at some horizon size, the temperature has a minimum. The temperature of the black hole becomes smaller as $|w|$ increases from $\frac{1}{3}$ to 1 for large enough black holes (big r_+), while it becomes larger for small r_+ . Thus large black holes radiate less for large $|w|$, while small black holes radiate more. Thus large black holes seem to be longer lived for large $|w|$.

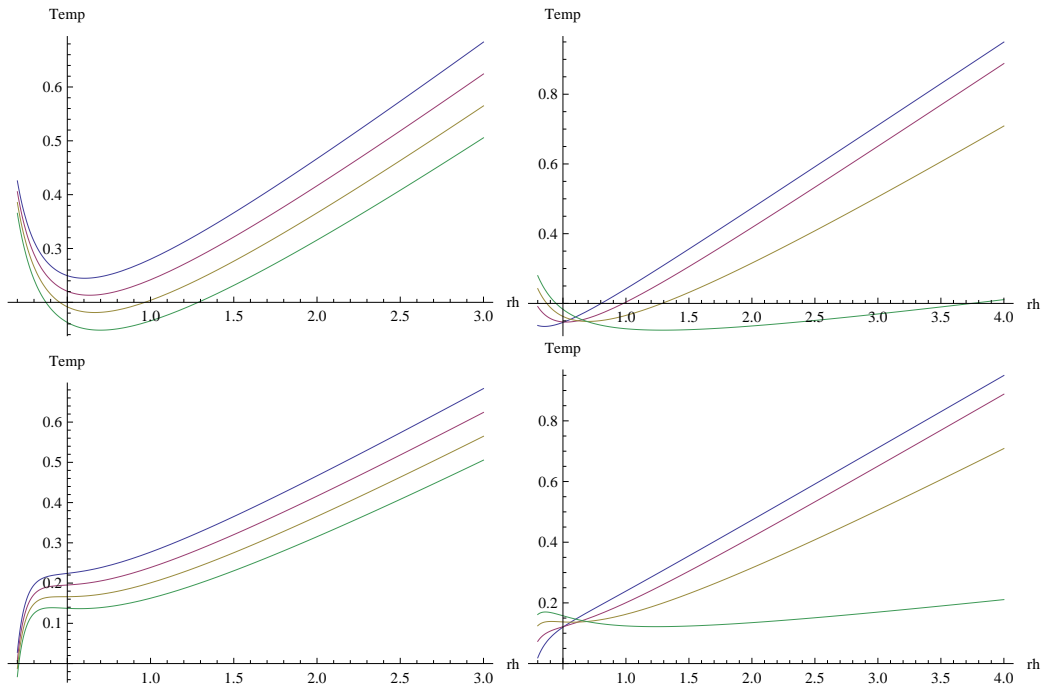


FIG. 2: (a) Temperature versus $r_h \equiv r_+$ for $Q = 0.00$, $w = -0.80$ and $a = 0.20$, (blue curve) $a = 0.40$ (purple curve) $a = 0.60$ (brown curve) and $a = 0.80$ (khaki curve). (b) Temperature versus $r_h \equiv r_+$ for $Q = 0.00$, $a = 0.80$ and $w = -0.40$, (blue curve) $w = -0.60$ (purple curve) $w = -0.80$ (cyan curve) and $w = -1.00$ (cyan curve). (c) Temperature versus $r_h \equiv r_+$ for $Q = 0.00$, $w = -0.80$ and $a = 0.20$, (blue curve) $a = 0.40$ (purple curve) $a = 0.60$ (brown curve) and $a = 0.80$ (cyan curve). (d) Temperature versus $r_h \equiv r_+$ for $Q = 0.00$, $a = 0.80$ and $w = -0.40$, (blue curve) $w = -0.60$ (purple curve) $w = -0.80$ (brown curve) and $w = -1.00$ (cyan curve).

IV. REGGE-WHEELER POTENTIALS

We first consider the metric in the AdS spacetime with quintessence

$$ds^2 = -f(r)dt^2 + \frac{dr^2}{f(r)} + r^2 d\Omega^2, \quad f(r) = 1 - \frac{2M}{r} + \frac{Q^2}{r^2} + r^2 - \frac{a}{r^{1+3w}}. \quad (31)$$

We concentrate specifically on the potential for scalar and gravitational perturbations. The potential with zero spin V_0 for scalar perturbations read

$$V_0 = f(r)g_0(r), \quad g_0(r) = \frac{f'(r)}{r} + \frac{l(l+1)}{r^2} = 2 - \frac{2Q^2}{r^4} + \frac{2M}{r^3} + \frac{l(l+1)}{r^2} + \frac{a(1+3w)}{r^{3+3w}}. \quad (32)$$

We start in Fig. 3, left panel, with the Regge-Wheeler potentials, when $a = 0$, so that quintessence plays no role at all; we set $M = 0.05$ and let Q take the values 0.00, 0.04, 0.07 and 0.10. It is obvious that, as Q increases, the left barrier of the potential becomes smaller, and at $Q = 0.10$ it disappears completely. In this case it is obvious that the potential cannot support bound states: any scalar excitation will end into the black hole horizon. This characteristic is independent from the role of quintessence. We continue in the right panel with the case $a = 0.8$, $w = -0.80$ and $M = 0.05$ and the same values for the charge Q as before. The picture is qualitatively the same, but the presence of the quintessence tends to reduce the size of the potentials.

We go ahead in Fig. 4 with the potentials for four different values of w , namely -0.40 , -0.60 , -0.80 , -1.00 , while $l = 0$, $M = 0.05$, for $Q = 0.00$ (left panel) and $Q = 0.04$ (right panel). We observe that, for both values of the charge,

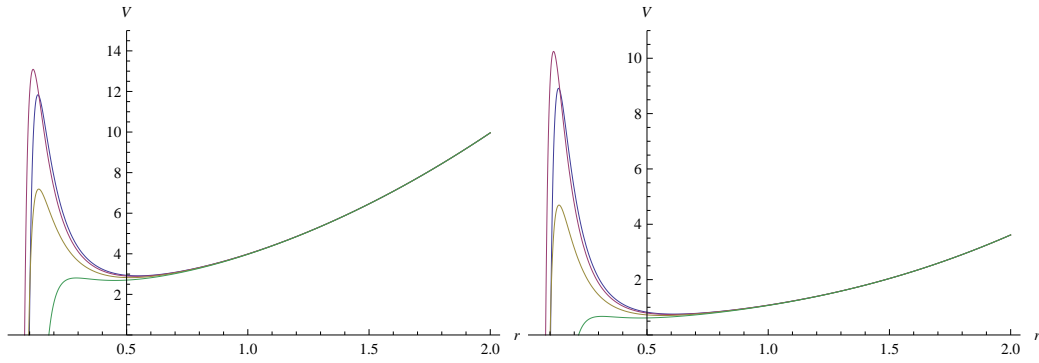


FIG. 3: Left panel: Potentials for $a = 0$, $l = 0$, $M = 0.05$ and four values of the charge: $Q = 0.00$ (pink curve), 0.04 (blue curve), 0.07 (khaki curve) and 0.10 (green curve). Right panel: Potentials for $a = 0.8$, $w = -0.80$, $M = 0.05$ and $Q = 0.00$ (pink curve), 0.04 (blue curve), 0.07 (khaki curve) and 0.10 (green curve).

the potential for $w = -0.40$ does not support bound states, but a left barrier gradually develops, as $|w|$ increases and bound states become possible.

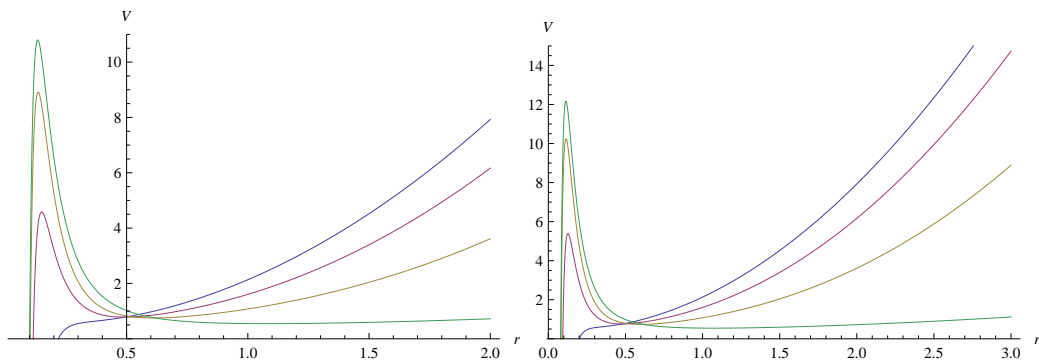


FIG. 4: Left panel: Potentials for $a = 0.8$, $l = 0$, $M = 0.05$, $Q = 0.00$, and four values for the parameter w : $w = -0.40$ (blue curve), -0.60 (pink curve), -0.80 (khaki curve) and -1.00 (green curve). Right panel: Same as in the left panel, but $Q = 0.04$.

Fig. 5, left panel, depicts potentials for $M = 0.05$, $Q = 0.00$, $w = -0.60$ and $l = 0, 1, 2$. It clearly shows that the presence of angular momentum builds gradually a barrier on the left, so that more bound states may be formed. On the other hand, in the right panel one may inspect the potentials for $M = 0.05$, $Q = 0.00$, $l = 0$, $w = -0.60$ and $a = 0.2, 0.4, 0.6, 0.8$.

V. FORMATION OF BOUND STATES

We now proceed with the calculation of the masses of the bound states, along with their imaginary parts. The latter signal the instability of these states, since they may tunnel through the barrier on the left and end up inside the horizon. To find the real part of the masses we follow [1] and consider the equation:

$$\int_{r_2}^{r_3} \frac{\sqrt{\omega^2 - V_0}}{f(r)} dr = \left(n + \frac{1}{2}\right) \pi, n = 0, 1, 2, \dots \quad (33)$$

and we tune ω , so that the equation is satisfied for some integer n . The states with $n = 0$ are the fundamental massive modes, while the ones with $n = 1, 2, \dots$ are the overtones. In general a small number of overtones exists. We also consider various values of the angular momentum quantum number l ; we will show the results for $l = 0$ and $l = 1$.

To determine the imaginary parts of these states, interpreted as bandwidths, we fix the value of ω that we found

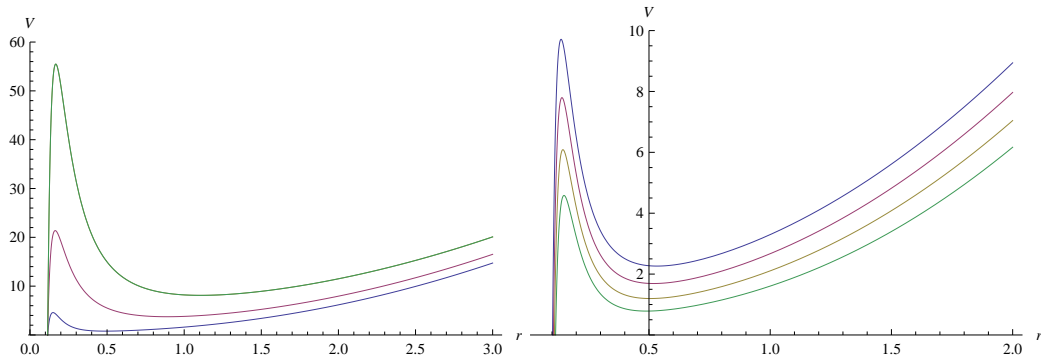


FIG. 5: Left panel: Potentials for $a = 0.8$, $M = 0.05$, $Q = 0.00$, $w = -0.60$ and three values for the angular momentum: $l = 0$ (blue curve), $l = 1$ (pink curve), and $l = 2$ (green curve). Right panel: Potentials for $l = 0$, $M = 0.05$, $Q = 0.00$, $w = -0.60$ and four values for the parameter a : $a = 0.2$ (blue curve), $a = 0.4$ (pink curve), $a = 0.6$ (khaki curve), and $a = 0.8$ (green curve).

in the previous step (call it $\tilde{\omega}$ say), and we calculate the bandwidth via:

$$\gamma = \tilde{\omega} \frac{\exp\left(-2 \int_{r_1}^{r_2} \frac{\sqrt{V_0 - \tilde{\omega}^2}}{f(r)} dr\right)}{1 + \exp\left(-\frac{2\pi p^2(r_{max})}{\sqrt{2 \frac{d^2 p^2(r_{max})}{dr_*^2}}}\right)}. \quad (34)$$

Notice that $\frac{d}{dr_*} = f(r) \frac{d}{dr}$, so that

$$\frac{d^2(p^2)}{dr_*^2} = f^2(r) \frac{d^2(p^2)}{dr^2} + f(r)f'(r) \frac{d(p^2)}{dr}, \quad p^2 = \tilde{\omega}^2 - V_0. \quad (35)$$

Notice that r_1 and r_2 are the two points common to the horizontal line at $\tilde{\omega}^2$ and the potential V_0 , which lie nearest to the origin, where the $\tilde{\omega}$ horizontal line cuts the potential curve, while r_3 is the most distant cut. In addition, r_{max} is the point, where the potential attains its maximal value. After we are done with these calculations, we have the mass eigenvalues in the form $\tilde{\omega} - i\gamma$.

We now report the mass eigenvalues and their bandwidths for various values of w and a . In Fig. 6, left panel, we depict the dependence of the masses on w for $Q = 0.00$, $M = 0.05$, $a = 0.8$ and $l = 0$. It appears that there exist no bound states for $|w|$ smaller than some value (about 0.55), while the bandwidths (denoted by error bars) increase as we approach this value. The masses do not change much, unless near the value $w = -1$. In the right panel we show the corresponding results for $Q = 0.00$, $M = 0.05$, $w = -0.6$ and $l = 0$. There is an almost linear dependence of the masses on a , while the bandwidths are more or less constant.

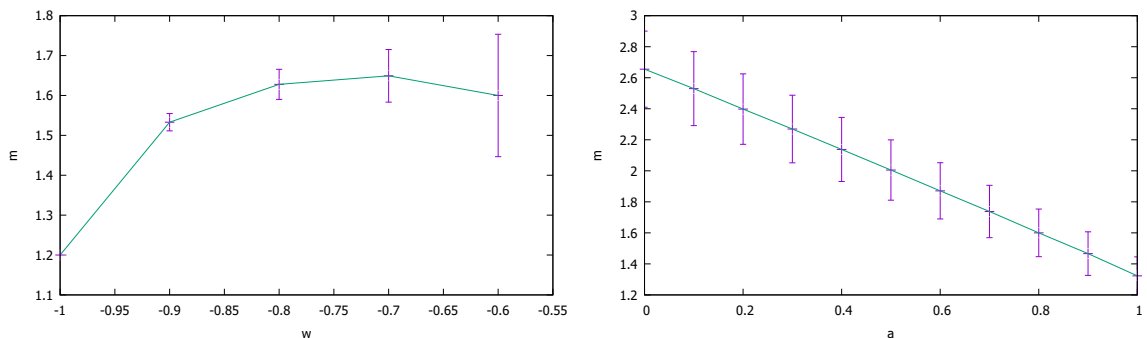


FIG. 6: Left panel: Masses versus w for $l = 0$. Right panel: Masses versus a for $l = 0$.

In Fig. 7, left panel, we depict the dependence of the masses on w for $Q = 0.00$, $M = 0.05$, $a = 0.8$ and $l = 1$. This larger angular momentum allows for eigenvalues for values of w smaller than before. In addition the bandwidths

are very much smaller and this is due to the large barrier on the left due to the angular momentum (compare Fig. 5); this barrier does not allow the particles go into the horizon easily, thus their imaginary parts are reduced to the size of the symbols. The masses are larger than before and the qualitative behaviour versus w is the same. In the right panel we depict the corresponding results for $Q = 0.00$, $M = 0.05$, $w = -0.6$ and $l = 1$. The dependence of the masses on a , is once more linear.

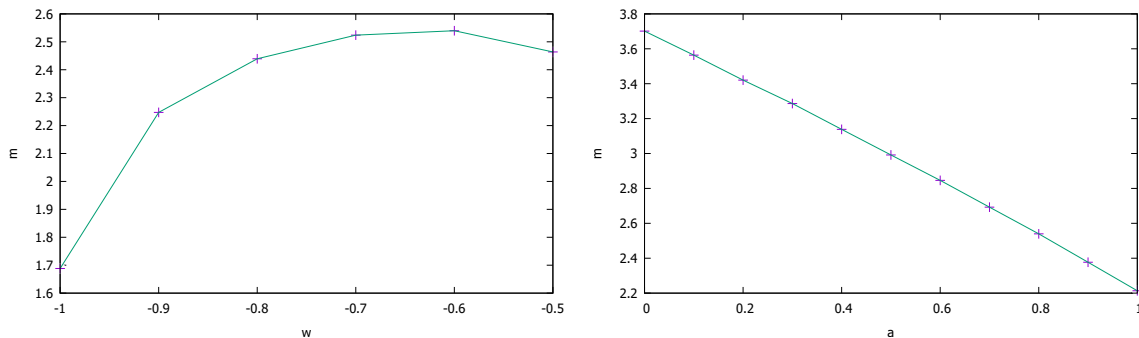


FIG. 7: Left panel: Masses versus w for $l = 1$. Right panel: Masses versus a for $l = 1$.

VI. CONCLUSIONS

We have studied black hole solutions in the presence of quintessence. In particular we concentrated in the bound states of scalar excitations outside the horizon. It has been shown that the parameters of the quintessence influence significantly the metric function and the Hawking temperature. It has turned out that large black holes radiate less for large $|w|$, while small black holes radiate more. Thus large black holes seem to be longer lived, compared to the ones with no quintessence for large $|w|$.

The Regge-Wheeler potentials depend on the charge Q of the black hole: when Q gets large enough, there is no left barrier, so the scalar particles will meet no obstacle to dive into the black hole. This has nothing to do with the quintessence. The presence of quintessence confines them to smaller values in general, although the qualitative picture of the Q dependence does not change. For small enough Q the presence of the quintessence may induce qualitative changes: the potential for $w = -0.40$ does not support scalar bound states, but increasing $|w|$ may create a potential with a barrier on the left, which can support bound states.

A barrier on the left may also be enhanced by increasing the angular momentum quantum number l . This suggests that the scalar particles with large angular momentum are longer lived than the ones with smaller l . The study of the potentials suggest that $|w|$ should be larger than some bound, if bound states are to be supported. On the other hand the masses decrease for increasing parameter a almost linearly. Also, the states with large angular momenta l have larger masses and smaller bandwidths than the ones with small l .

-
- [1] J. Grain and A. Barrau, Eur. Phys. J. C **53**, 641-648 (2008) [arXiv:hep-th/0701265 [hep-th]].
 - [2] A. Barrau, N. Ponthieu, Phys. Rev. D **69** (2004) 105021.
 - [3] B. J. Carr, [arXiv:astro-ph/0511743 [astro-ph]].
 - [4] T. Begge and J. A. Wheeler, Phys. Rev. **108**, 1063 (1957)
 - [5] M. Calzá, 2502.04041 (2025)
 - [6] G. Koutsoumbas, I. Mitsoulas and E. Papantonopoulos, Class. Quant. Grav. **35**, no.23, 235016 (2018) [arXiv:1803.05489 [gr-qc]].
 - [7] T. Kolyvaris, G. Koutsoumbas, E. Papantonopoulos and G. Siopsis, Class. Quant. Grav. **29**, 205011 (2012) [arXiv:1111.0263 [gr-qc]].
 - [8] M. Rinaldi, Phys. Rev. D **86**, 084048 (2012) [arXiv:1208.0103 [gr-qc]].
 - [9] T. Kolyvaris, G. Koutsoumbas, E. Papantonopoulos and G. Siopsis, JHEP **11**, 133 (2013) [arXiv:1308.5280 [hep-th]].
 - [10] A.G. Riess, et al., Ap.J. **607**, 665 (2004), A. G. Riess et al., Astronom. J. **116**, 1008 (1998).
 - [11] S. J. Perlmutter et al., Astrophys. J. **517**, 565 (1999).
 - [12] S. M. Carroll, Living Rev. Relativ. **4**, 1 (2001).

- [13] E. J. Copeland, M. Sami, S. Tsujikawa, *Int. J. Mod. Phys. D* **15**, 1753 (2006).
- [14] S. Hellerman, N. Kaloper and L. Susskind, *JHEP* **0106**, 003 (2001) [arXiv:hep-th/0104180];
W. Fischler, A. Kashani-Poor, R. McNees and S. Paban, *JHEP* **0107**, 003 (2001) [arXiv:hep-th/0104181].
- [15] T. Banks, W. Fischler and L. Motl, *JHEP* **9901**, 019 (1999) [arXiv:hep-th/9811194];
T. Banks, arXiv:hep-th/0011255;
T. Banks and W. Fischler, arXiv:hep-th/0102077.
- [16] E. Witten, [arXiv:hep-th/0106109 [hep-th]].
- [17] S. Hellerman, N. Kaloper, L. Susskind, *J. High Energy Phys.* **06**, 003 (2001).
- [18] V. V. Kiselev, *Class. Quant. Grav.* **20**, 1187-1198 (2003) [arXiv:gr-qc/0210040 [gr-qc]].
- [19] S. Chen, B. Wang, R. Su, *Phys. Rev. D* **77**, 124011 (2008).
- [20] S. Dutta and R. J. Scherrer, *Phys. Rev. D* **78**, 123525 (2008) [arXiv:0809.4441 [astro-ph]].
- [21] K. Bamba, S. Capozziello, S. Nojiri and S. D. Odintsov, *Astrophys. Space Sci.* **342**, 155 (2012).
- [22] K. Ghaderi, B. Malakolkalami, *Grav. Cosmol.* **24**, 61 (2018).
- [23] H. Chen, B. C. Lutfuoglu, H. Hassanabadi, Z. W. Long, *Phys. Lett. B* **827**, 136994 (2022).
- [24] B. Hamil, B. C. Lutfuoglu, *Eur. Phys. J. Plus* **137**, 1124 (2022).
- [25] R. Wang, F. Gao, H. Chen, *Phys. Dark Universe* **40**, 101189 (2023).
- [26] B. Hamil, B. C. Lutfuoglu, *Phys. Dark Universe* **44**, 101484 (2024).
- [27] J. D. Bekenstein, *Phys. Rev. D* **7**, 2333 (1973).
- [28] S. W. Hawking, *Phys. Rev. D* **13**, 191 (1976).